

ANALYSIS OF FLOW STRUCTURES AROUND STATIONARY AND OSCILLATING SQUARE CYLINDERS

Yongxin Chen
Engineering and Physical
Sciences
University of Southampton
Southampton, UK, SO17 1BJ
y.chen@soton.ac.uk

Zheng-Tong Xie
Engineering and Physical
Sciences
University of Southampton
Southampton, UK, SO17 1BJ
z.xie@soton.ac.uk

Kamal Djidjeli
Engineering and Physical
Sciences
University of Southampton
Southampton, UK, SO16 7QF
kkd@soton.ac.uk

ABSTRACT

Flow past stationary and oscillating square cylinders at Reynolds number 22,000 are studied by using large eddy simulation (LES). The square cylinder is forced to oscillate at the resonance frequency. The effect of small amplitude motion on aerodynamics is compared with that of a stationary cylinder in smooth incoming flow. It is found the oscillation triggers earlier reattachment on the side surfaces of cylinder. Consequently, a more chaotic pressure field is generated downstream the reattachment point and more upstream reverse flow is generated via the flow entrainment from the free shear layer. In addition, effect of free stream turbulence on the stationary square cylinder are investigated at the same Reynolds number. Different turbulence intensities and integral length scales are tested. It is found that the incoming turbulence evidently increases the length of recirculation region in the wake, and reduces the surface pressure fluctuations on the side surfaces compared to those in a smooth incoming flow. POD analysis is used to compare the contribution of each mode between smooth and turbulent incoming flows, and confirms that the incoming turbulence with the integral length scale equal to the square cylinder side length elongates the recirculation region in the wake. This is because the contribution from the most energetic modes of the turbulent inflow to the primary flow around the square cylinder is through superposing structures with length scale larger than the cylinder side length.

Introduction

A square cylinder is one of simple geometries that is used to understand mechanism of turbulent flow past a bluff body. To analyse the flow structures around a square cylinder, this paper consists of two parts. In the first part, the inlet velocity is chosen to be constant, i.e. smooth inflow. Flow past a square cylinder at Reynolds number based on free stream velocity U_0 and side length of square cylinder D at 22,000 is studied for both stationary and oscillating cylinder cases. For the oscillating cylinder cases, a sinusoidal motion of the cylinder is prescribed. Two amplitude ratios A/D of 0.05 and 0.1 are selected. The reduced velocity $U_r = U_0/(ND)$ for both oscillating cases is chosen to 7.7 which is referred to the resonance point (Bearman & Obasaju, 1982). These are reported in Chen *et al.* (2019), and only a very small selection of data is presented here.

In the second part, an incoming flow with free stream

turbulence is imposed at the inlet. The effect of free stream turbulence on a stationary square cylinder is studied. The Reynolds number is the same as in the first part.

Numerical methods

An efficient and accurate finite volume incompressible flow solver with a staggered arrangement in the Cartesian grid has been developed to simulate turbulent flow past a moving bluff body. Second order Adam-Bashforth method is used for temporal discretisation. Central difference scheme and QUICK scheme are used for diffusion term and convection term respectively. The sub-grid scale (SGS) term of the governing equations of large-eddy simulation (LES) is modelled using the mixed time scale model (Inagaki *et al.*, 2005). To simulate flow around a bluff body, an efficient immersed boundary method (Yang & Balaras, 2006) is implemented to model solid structures in the Cartesian grid, which substantially simplifies the mesh generation for complex geometries.

The computational domain size for all cases is $27D \times 20D \times 4D$ in streamwise, cross-stream and spanwise directions respectively. The centre of the cylinder is placed on the origin of computational domain, from where the distances to the inlet and outlet are $7D$ and $20D$ respectively.

For boundary conditions, two types of inlet conditions are used for the two parts respectively. In the first part, a uniform velocity is imposed at the inlet. In the second part, synthetic turbulence is generated (Xie & Castro, 2008) and imposed at the inlet. To reduce the computational cost, the turbulent inflow plane is only applied from $y/D=-1.5$ to 1.5 , where the free shear layers over the side surfaces of square cylinder downstream are completely accommodated. Zero gradient boundary conditions are used at the outlet. Symmetric boundary conditions are used for the top and bottom boundaries. Periodic boundary conditions are used in the spanwise direction. No-slip boundary conditions are applied on the surfaces of the square cylinder using the immersed boundary method. Uniform mesh is used in solid body region and mesh is stretched toward far fields. 200 points are used to resolve one side of the square cylinder. y_1^+ based on the local wall shear stress is less than 5. The maximum CFL number for all cases is less than 0.3.

The prescribed motion of the square cylinder is defined as $y(t) = A \sin(2\pi Nt)$, where A and N are respectively amplitude and frequency of the prescribed motion, t is time.

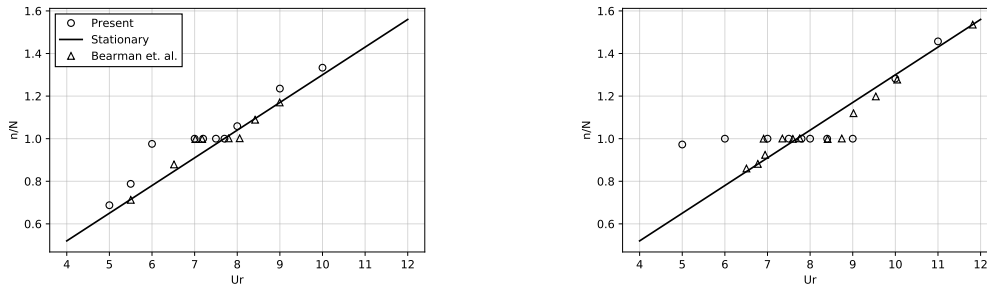


Figure 1. Shedding frequency versus reduced velocity. Left: $A/D = 0.05$; Right: $A/D = 0.1$. The straight line is the n/N vs Ur relationship of a stationary cylinder.

Reduced velocity $U_r = U/(ND) = 7.7$, which is within the resonance frequency range, is chosen. For a comparison with the experimental data (Bearman & Obasaju, 1982), two amplitudes $A/D = 0.05$ and 0.1 are chosen. To obtain converged statistics, data of 15 vortex shedding periods are sampled in stationary cylinder cases, and data of 12 complete cycles of oscillations are sampled in moving cylinder cases.

Flow past stationary and oscillating square cylinders

Figure 1 shows our numerical data of the relationship between vortex shedding frequency and reduced velocity for two amplitude ratios of an oscillating square cylinder against the experimental data (Bearman & Obasaju, 1982). The lock-in region is captured for both amplitude ratios. In lock-in region, the vortex shedding is synchronized with cylinder motion, consequently surface stress and flow features are changed. By investigating the flow past the stationary and oscillating square cylinders, similarities and difference are analyzed, and flow features are carefully examined and compared in terms of surface forces and flow characteristics.

Figure 2 shows a comparison of probability density function (PDF) distribution of surface pressure fluctuations at four locations $x/D=0, 0.2, 0.4$ and 0.45 , on the upper side surface. The result of amplitude ratio $A/D = 0.1$ is similar with the smaller amplitude case ($A/D = 0.05$). Only the stationary case and the oscillating cylinder case at amplitude ratio $A/D = 0.05$ are shown here. For the stationary case, all of the PDFs at the four stations evidently show a double-peak distribution. A similar double-peak distribution is also found on the upstream half of side surfaces (not shown here). The double-peak distribution on the side surfaces is consistent with the observation in Yu & Kareem (1996). For the oscillating cylinder cases, the double-peak distribution occurs from the leading edge downstream up to approximately $x/D = 0.2$. From $x/D = 0.2$ downstream, the double-peak distribution gradually disappears, and a single-peak distribution occurs at $x/D = 0.45$ near trailing edge. The double-peak distribution of pressure fluctuation suggests that positive and negative pressure fluctuations alternate on the upper surface. This is primarily due to the alternating vortex shedding on the two side surfaces. For the stationary cylinder, flow separates from the leading edge and may reattach in near trailing edge region. During this procedure, vortices convect and merge or break into smaller ones over the side surfaces. On the contrary, a narrow-banded PDF distribution (i.e. the single-peak distribution) indicates

that the pressure fluctuations are more random and less coherent than the double-peak distribution.

An array of probes are placed on the upper side face to record the wall shear stress. In the streamwise direction, more than 100 rows are equally spaced, while in the spanwise direction 60 columns are equally spaced. Figure 3 shows a comparison of spanwise averaged wall shear stress on the upper side surface of stationary and oscillating cylinder ($A/D = 0.05$) over one complete sinusoidal cycle of lift. Again it is to be noted that the results of the two oscillating cylinders are similar. The horizontal axis of Figure 3 is the time over one period, while the vertical axis shows the location of the evenly distributed probes in the streamwise direction from the leading edge ($x/D = -0.5$) to the trailing edge ($x/D = 0.5$) on the upper surface. The oscillating cylinder case shows a larger area with a large variation than that of the stationary cylinder case. It is noted that the large variation of shear stress shows a negative sign, which denotes reverse flow. Figure 3 shows that the reverse flow occurs only from the middle of upper surface downstream for the stationary cylinder case, whereas it reaches further upstream close to the leading edge for the oscillating cylinder case. The variations of shear stress mainly cluster just downstream of the middle of upper surface for the stationary cylinder case. In contrast, the primary variations for the oscillating cylinder case occurs upstream of the middle of the upper surface. This comparison confirms that the oscillation of the cylinder significantly affects the flow behaviour in the near wall region.

Effect of free stream turbulence with a stationary square cylinder

In this section, the results of flow past a stationary square cylinder at Reynolds number 22,000 in a free stream turbulent flow are presented. Three combinations of turbulence intensities (TI) and integral length scales (ILS) are investigated. The results are compared against those of smooth incoming flow cases. The TI is defined as $\sqrt{\frac{2}{3}k}/U_0$, where k is turbulent kinetic energy. The ILS is chosen assuming that the free stream turbulence is isotropic and homogeneous. Three combinations of turbulent incoming flow are (1) $TI=0.04, ILS = 1D$; (2) $TI=0.04, ILS = 0.2D$; (3) $TI=0.10, ILS = 0.2D$.

Figures 4 and 5 show the contours of time and spanwise averaged Reynolds normal stresses $\langle \overline{u'u'} \rangle$ and $\langle \overline{v'v'} \rangle$ of incoming turbulent flow cases against those of smooth incoming flow case. Figure 4 shows the overall strength of $\langle \overline{u'u'} \rangle$ is reduced for the incoming turbulent

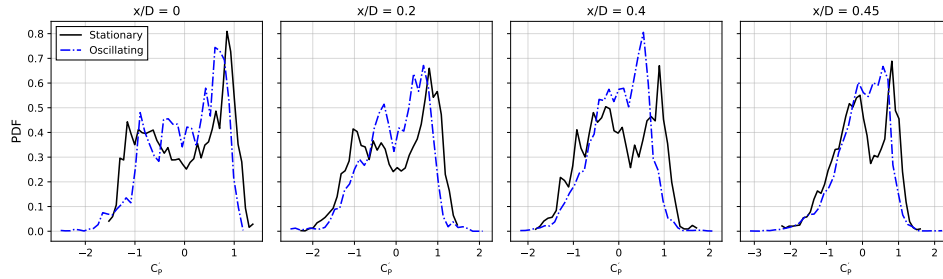


Figure 2. Comparison of normalized PDF of pressure fluctuations on the upper surface. The columns from left to right are for the locations at $x/D = 0, 0.2, 0.4$ and 0.45 respectively.

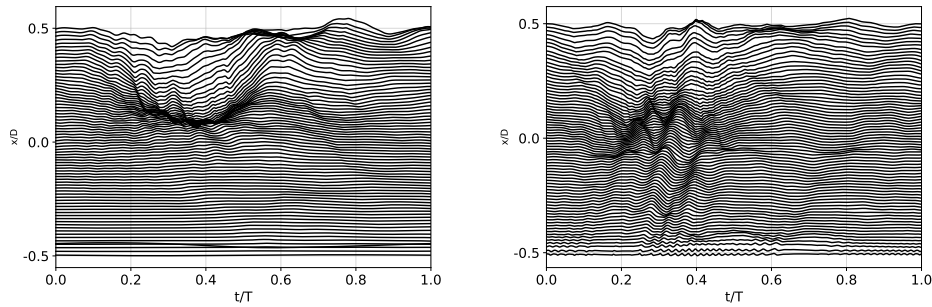


Figure 3. Comparison of spanwise-averaged wall shear stress on the upper surface over one complete sinusoidal cycle of lift. Left: stationary cylinder, Right: oscillating cylinder at amplitude ratio $A/D=0.05$.

flow cases than that for the smooth incoming flow case, especially in the near trailing edge region on the side surfaces and the recirculation region in the wake. At this Reynolds number, flow separates from the leading edge and reattaches on the side surfaces. The region near the trailing edge with a higher $\langle \overline{u'u'} \rangle$ denotes a greater oscillation of the separation the reattachment on the side surfaces. From (a) to (c), the strength of oscillation of the separation and the reattachment on the side surfaces is weakened as the incoming flow changes from smooth to turbulent. From (c) to (b), the *ILS* of the incoming turbulence increases, while the strength of $\langle \overline{u'u'} \rangle$ in the flow reattachment region over the side surface is in no evident change. Nevertheless, Figure 4(b) shows a longer spread in the wake than that for the smaller *ILS* in Figure 4(c). Figure 4(c) and (d) show that an increase of the *TI* results in a weaker oscillation of the separation both in the shear layer and wake. The recirculation region in the wake is longer in turbulent incoming flow than that in smooth incoming flow. This is consistent with Tamura & Ono (2003).

$\langle \overline{v'v'} \rangle$ shown in Figure 5 quantifies the strength of variation of flow in vertical direction. It can also indicate flow entrainment and vortex forming in the wake region. Figure 5 shows consistent flow behaviour as that in Figure 4 in term of inflow turbulence effect. The magnitude of Reynolds normal stress $\langle \overline{w'w'} \rangle$ is in one order smaller than those of Reynolds normal stresses $\langle \overline{u'u'} \rangle$ and $\langle \overline{v'v'} \rangle$. The change of $\langle \overline{w'w'} \rangle$ is less evident compared to the other two Reynolds normal stresses.

Figure 6 shows a comparison of power spectrum density (PSD) of cross-stream component v in the wake region between smooth and turbulent cases. Two monitor points in the wake region on the middle plane ($y = 0$) are selected and they are on $x/D = 1$ and $x/D = 2$. An inertial sub-layer with a $-5/3$ slope is evident in both cases. The Strouhal num-

bers of the vortex shedding of the two cases, which correspond to the primary peaks of spectra, are different for the two cases. It is 0.133 for the smooth incoming flow case, differs from 0.129 for the incoming turbulent flow case. A smaller shedding frequency corresponds to a slower oscillation of recirculation, and is consistent with a greater length of recirculation region. These confirm the data shown in Figures 4 and 5 and relevant discussions.

Coherent structures of a stationary square cylinder in smooth and turbulent incoming flows

To further examine the effect of free stream turbulence, we compare flow structures of the smooth and turbulent incoming flow cases using the proper orthogonal decomposition (POD) method. POD is modal decomposition technique that extracts most energetic modes. This method is useful to identify coherent structures from a complicated turbulent flow field. The turbulent incoming flow used to compare is with $TI = 0.04$ and $ILS = 1D$, and is denoted as turbulent case hereafter.

In current study, the non-dimensional time interval $\Delta TU_0/D = 0.1$ between two continuous snapshots is used. Sensitivity tests are performed using different numbers of snapshots, in which 400, 500 and 600 snapshots are taken from both smooth and turbulent incoming flow cases after the flows are fully developed. The difference between the three sets of POD results is negligible. The three sets of POD results are considered being converged, and the set calculated from 500 snapshots are presented hereafter.

Figure 7 shows the comparison of normalized eigenvalues of POD modes of the entire flow field between smooth and turbulent incoming flow cases. The first two modes account for nearly 60% of total energy. The first 40 modes

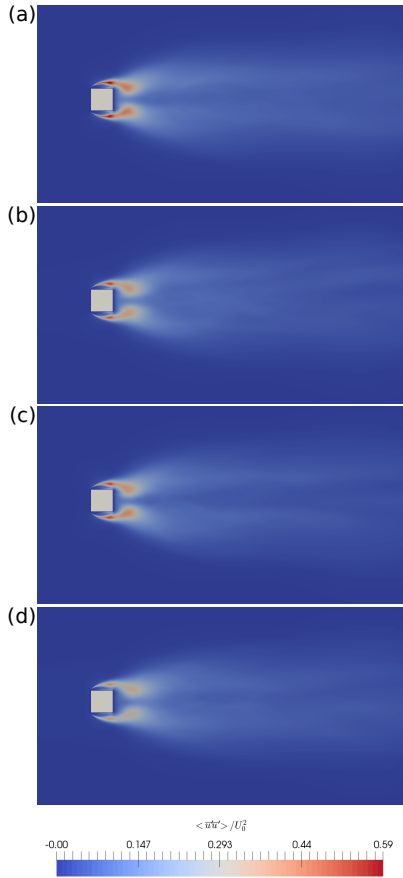


Figure 4. Comparison of normalized time and spanwise averaged Reynolds normal stress $\langle \overline{u'u'} \rangle$. From top to bottom: (a) smooth inlet; turbulent inlet with (b) $ILS = 1D$, $TI = 0.04$; (c) $ILS = 0.2D$, $TI = 0.04$; (d) $ILS = 0.2D$, $TI = 0.10$.

account for over 90% of total energy, by which we consider flow can be well represented and reconstructed. The first two modes show similar energy contributions to the flow field because the periodic vortex shedding is the dominant flow motion in these cases. The travelling structures are represented by a pair of POD modes, which are spatially similar but shifted (Taira, 2017). The eigenvalues of the same 'rank' mode show a similar result between smooth and turbulent incoming flow cases. This suggests that the incoming flow with a small turbulence intensity has only a small impact on the energy distribution of flow structures.

Figure 8 shows the comparison of 1st, 20th and 40th POD modes and results are shown by streamwise velocity component u , where λ_x denotes the wavelength of incoming turbulence structure. The similar energy contribution of the same 'rank' mode shown in Figure 7 reflects in Figure 8, where the shape and size of structures in the wake are similar between the corresponding modes. In the 1st mode, a clear anti-symmetric structure is evident in the wake, which corresponds to the Karman-vortex shedding. However, it is rather difficult to distinguish the structures and their physical significances in 20th and 40th modes. Through the POD modes, the wavelength λ_x of the incoming turbulence structures can be qualitatively estimated. λ_x decreases continuously as the rank of mode decreases. The length scale of the 40th mode of the incoming turbulence structure is greater than the cylinder side length D .

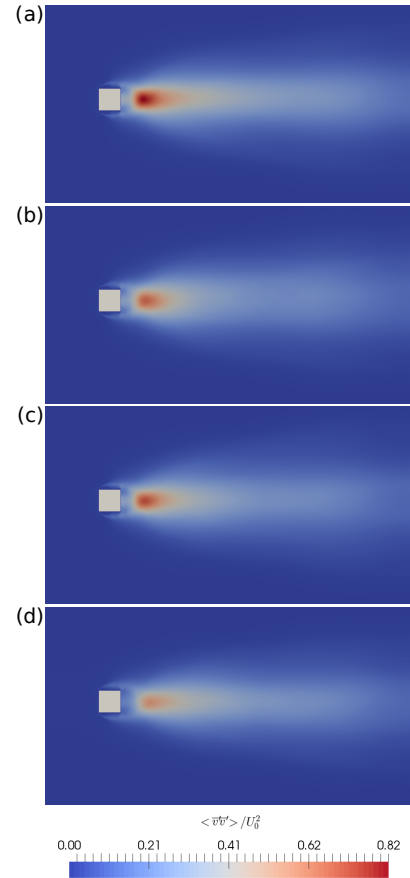


Figure 5. Comparison of normalized time and spanwise averaged Reynolds normal stress $\langle \overline{v'v'} \rangle$. The order of each subplot is identical with Figure 4.

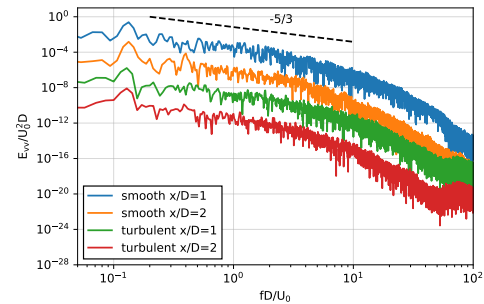


Figure 6. Comparison of power spectra of cross-stream velocity component v in the wake region between smooth and turbulent case with $ILS = 1D$, $TI = 0.04$.

Through the POD analysis, the mechanism of the inflow turbulence effect on flow around a square cylinder is further understood. For the current inflow turbulence integral length scales, we understand that the contribution (or perturbation) from the most energetic modes in the turbulent inflow to the primary flow around the square cylinder is through superposing structures (or waves) with length scales greater than the cylinder side length D . These waves pass around the cylinder and elongate structures in the wake. Consequently the recirculation region in the wake is elongated. This confirms the findings by using Reynolds stress (Figure 5).

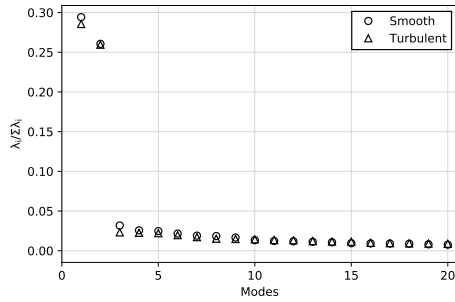


Figure 7. Comparison of normalized eigenvalues of POD modes.

In the above POD analysis, snapshots of velocity field consisting of the three velocity components of the whole domain are stacked for processing. In current configuration, the turbulent inflow is only applied from $y/D = -1.5$ to 1.5 , whereas the velocity field of most of the inflow is undisturbed. The POD analysis may be less effective if much of undisturbed area is included for processing. Moreover, compared to the vertical velocity component v , the streamwise velocity component u is less sensitive to change of flow conditions since the principal flow motion is in the streamwise direction. The effectiveness of the identification of coherent structures could be influenced if the streamwise velocity component is included (Mulleners *et al.*, 2008). Hence, we only use the vertical velocity component v data in the free shear layer region over the upper surface to examine the flow entrainment. A window $x/D \in [-0.6, 1.0]$ and $y/D \in [0.5, 1.0]$ is chosen in the free shear layer for POD analysis.

Figure 9 shows the comparison of eigenvalues of POD modes and their relative errors in smooth and turbulent incoming flow cases. Only one leading eigenvalue exists in the both cases rather than a pair of leading eigenvalues calculated from the whole domain data shown in Figure 7. The relative error in Figure 9 shows that the inflow turbulence has a negative impact on the contribution of first two modes, and a positive impact on that of the other modes. Figure 9 shows that with the introduction of incoming turbulence, the most energetic structures (i.e. the 1st and the 2nd modes) are weakened, whereas the less energetic structures are intensified. We speculate that incoming turbulence splits the large scale structures into smaller ones.

Figure 10 shows the comparison of time and spanwise averaged pressure and pressure fluctuation on the square section between smooth and turbulent inflow cases. The pressure coefficient are nearly the same in the two cases. As for the *r.m.s* of pressure fluctuations, Figure 10(right) shows that the C'_{prms} is greater on the windward surface in particular at the stagnation, but is less on the side and leeward surfaces compared to that in the smooth case. On the windward surface where the flow is attached, the greater C'_{prms} is due to the inflow velocity fluctuations in the turbulent inflow case. On the other hand, the incoming turbulence elongates the recirculation in the wake and weakens the overall flow entrainment shown in Figures 4 and 5, and the surface pressure fluctuations on the side and leeward surface are less accordingly. The POD analysis shows that in incoming turbulence the large scale vortices forming and travelling over the side surfaces are split into less energetic and smaller scale vortices. This causes the decrease of

surface pressure fluctuations on the side and leeward faces in the turbulent incoming flow case compared to smooth incoming flow case.

Conclusion

In this paper, smooth flow past stationary and oscillating square cylinders at Reynolds number 22,000 is studied. The motion of oscillating square cylinders is prescribed by a sinusoidal function at a reduced velocity 7.7, which corresponds to the resonance reduced velocity. Two amplitude ratios $A/D = 0.05$ and 0.1 are simulated to compare against the experiment data. The oscillation of the cylinder evidently changes pressure distribution particularly in the near trailing edge region. The probability distribution function (PDF) of surface pressure in the near trailing edge region is changed from a double-peak distribution in the stationary case to a single-peak distribution in the oscillating cylinder cases. These suggest that the vortex formation and shedding in the near trailing edge region are significantly affected by the oscillation of the cylinder. The instantaneous and time averaged shear stress show that the oscillation of the cylinder shifts the reattachment point of the reverse flow upstream evidently.

Incoming free stream turbulent flow past a stationary square cylinder at the same Reynolds number is studied, and shows a non-negligible effect to the flow around. The turbulent incoming turbulent flow weakens the oscillation of the recirculation and reattachment on the side surfaces, and causes less surface pressure fluctuations. Our POD analysis confirms these findings. The POD analysis shows that the incoming turbulence elongates the recirculation region in the wake, and causes a decrease of surface pressure fluctuations on the side and leeward faces compared to those in the smooth inflow.

REFERENCES

- Bearman, PW & Obasaju, ED 1982 An experimental study of pressure fluctuations on fixed and oscillating square-section cylinders. *JFM* **119**, 297–321.
- Chen, Y, Djidjeli, K & Xie, ZT 2019 Large eddy simulation of flow past stationary and oscillating square cylinders. *J Fluid Struct.* (under review).
- Inagaki, M, Kondoh, T & Nagano, Y 2005 A mixed-time-scale sgs model with fixed model-parameters for practical les. *J Fluids Eng.* **127** (1), 1–13.
- Mulleners, K, Hemireg, A & Raffel, M 2008 Investigations of a trailing edge stall on 2d airfoils. In *14th Int. Symp. App. Laser Tech. Fluid Mech.*
- Taira, K et al. 2017 Modal analysis of fluid flows: An overview. *AIAA Journal* pp. 4013–4041.
- Tamura, T & Ono, Y 2003 LES analysis on aeroelastic instability of prisms in turbulent flow. *J Wind Eng. Ind. Aerodyn.* **91** (12-15), 1827–1846.
- Xie, ZT & Castro, IP 2008 Efficient generation of inflow conditions for large eddy simulation of street-scale flows. *Flow Turbul. Combust.* **81** (3), 449–470.
- Yang, J & Balaras, E 2006 An embedded-boundary formulation for large-eddy simulation of turbulent flows interacting with moving boundaries. *JCP* **215** (1), 12–40.
- Yu, DH & Kareem, A 1996 Two-dimensional simulation of flow around rectangular prisms. *J Wind Eng. Ind. Aerodyn.* **62** (2-3), 131–161.

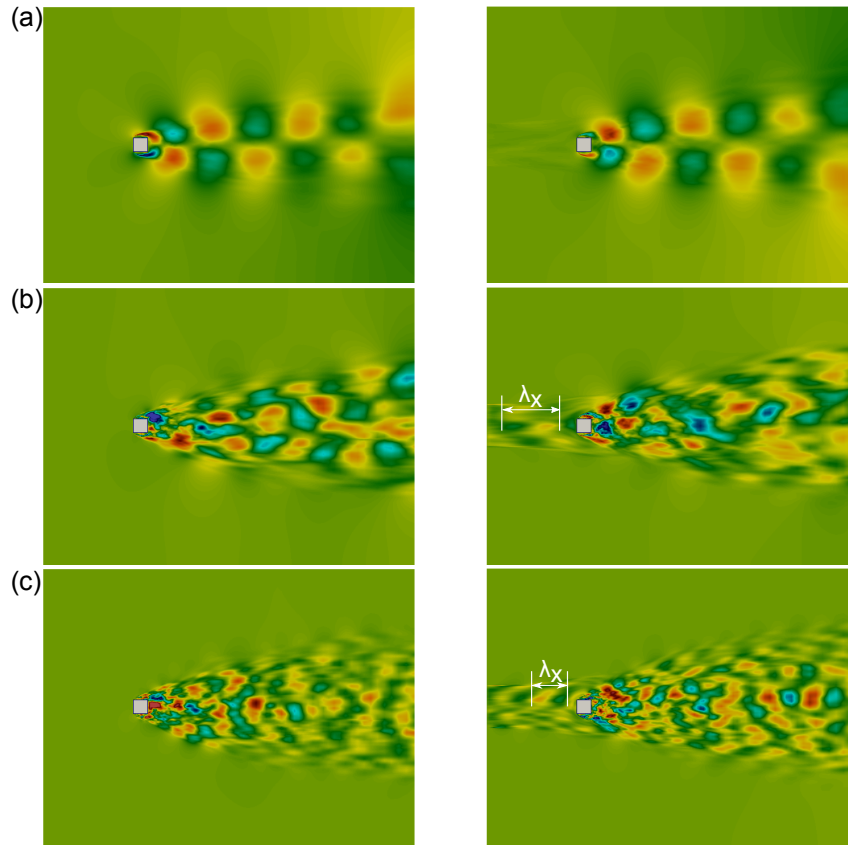


Figure 8. Comparison of streamwise velocity component u of POD modes between smooth (left) and turbulent (right, $ILS = 1D$, $TI = 0.04$) cases. (a) 1^{st} mode; (b) 20^{th} mode; (c) 40^{th} mode.

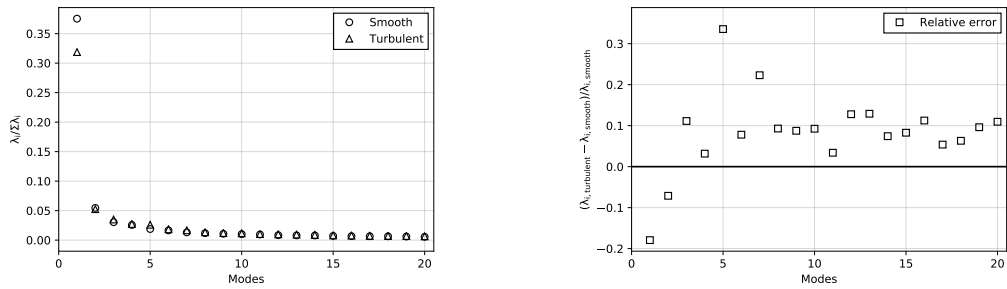


Figure 9. Comparison of eigenvalues of POD modes between smooth and turbulent ($ILS = 1D$, $TI = 0.04$) cases in free shear layer. Left: normalized eigenvalues; Right: relative errors of eigenvalues between each mode.

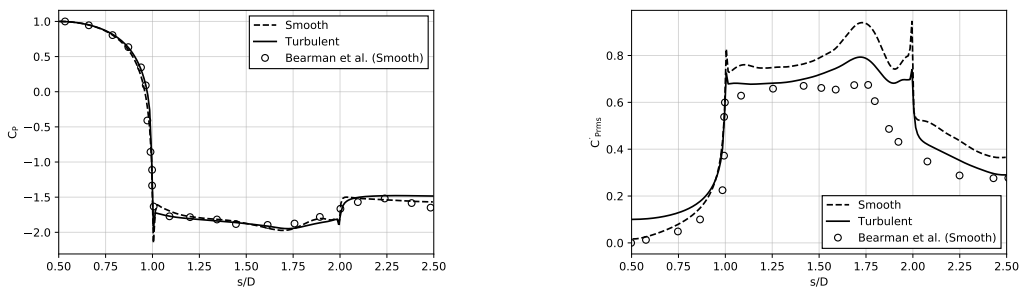


Figure 10. Comparison of distribution of pressure (left) and pressure fluctuation (right) over the circumferential direction of square section between smooth and turbulent ($ILS = 1D$, $TI = 0.04$) inlets.